Fracture modes in a triangular lattice crystal: Numerical and phenomenological studies

H. Furukawa
Faculty of Education, Yamaguchi University, Yamaguchi 753, Japan
(Received 19 June 1995)

By numerical simulations we study the stationary or terminal crack propagation in the triangular lattice system with a truncated harmonic potential under several static external stresses. For the external stress called mode I we found three typical crack propagation modes for the strong external stress, and one more mode for the weak external stress. These crack propagation modes are classified by the potential depth scaled by the external stress. Two of the modes are related to two sound modes: The regions by the transverse and the longitudinal sound modes are separated from each other. There is a supersonic mode by which the crack propagation velocity exceeds the sound velocity. Only in the weak stress case does a zigzag crack pattern appear. By this mode the crack propagation velocity is about half of the transverse sound velocity. We examined the zigzag crack surface and found that its roughness exponent is about 0.75, which is near to those observed experimentally. A system size dependence of the critical potential depth for the crack propagation is also found. Different external stresses (so-called mode II, mode III, and spherical stresses) are also examined. Sometimes different aspects for the fracture were seen, but they are explained by the same basic ideas that have been developed for mode I stress.

PACS number(s): 61.20.Ja, 81.40.Np, 46.30.Nz, 62.20.Mk

I. INTRODUCTION

The fracture mechanics provides with rich contents not only as a microscopic fundamental physics but also as a macroscopic physics [1]. For instance, time-dependent external stresses reveal periodic regular crack patterns [2–8], which are considered to belong to the class of the pattern forming irreversible phenomena seen widely in nature [9,10]. However, the fracture itself is a microscopic phenomenon and should be closely related to mechanical properties of the material. If the material is a perfect crystal, principal dynamical factors related to the fracture are the force constant, the particle mass and the crystal structure, which are just factors for the sound motion. Therefore, it is probable that the fractures are microscopic phenomenon closely related to the sound propagation. In fact several theoretical analyses suggested the equivalence between the crack propagation terminal velocity and (Rayleigh) sound velocity [11–14]. On the other hand, the experiment [15] and the numerical simulation [16] exhibit different features of fracture. Crack propagation velocities are about half of the sound velocity [15,16] and crack surfaces are generally fractals [17–20]. Such a fractal nature is not taken into consideration in the theoretical calculations of crack propagation velocity. It is probable that the fractal nature of the crack surface and the reduction of the crack propagation velocity should be closely related to each other, though we have no satisfactory explanation of the discrepancy between the theoretical and the experimental observations. Therefore, we need much more information on the crack propagation even for a simplified dynamical model. A complete information on crack propagation over a wide parameter range of a simplified model will help us to understand the nature of the crack propagation in a real system.

In this paper we shall extensively study the crack propagation using the numerical simulation for an idealized dynamical lattice model in two dimensions. Four types of external stresses, i.e., so-called mode I, mode II, mode III, and spherical stresses are examined. The fracture in the case of the mode I stress is examined in detail. We concentrate our attention on the stationary or terminal state of the crack propagation. We, therefore, do not pay much attention to the very early stage of the crack propagation [21]. Crack propagations are started under several initial conditions. To obtain global information on the crack propagation for the present model we study the simulation in wide ranges of values of parameters for the external stress and the interparticle potential depth. In a wide parameter range our study partly supports the theoretical prediction that the crack propagation velocities are approximately equal to sound velocities. But in contrast to the theoretical condition crack patterns are not regular, in general. Most of crack patterns are very complicated: They are often very irregular, multiply branched or zigzag. In the case of mode I stress we found three or four broad parameter regions for crack propagation velocity as a function of a reduced potential depth parameter. Two of them are related to the longitudinal and the transverse sound velocities, respectively. Origins of these regions are qualitatively explained. In the case of weak stress there is a region with a single zigzag crack pattern before the crack stops propagating. In this case the crack propagation velocity is by no means equal to the sound velocity. The crack propagation velocity is about half of the transverse sound velocity, and the crack surface is a fractal. The fracture mode in this case resembles that in the case where dynamical fractures have been examined by experiments [15] and a realistic

 ©1995 The American Physical Society

numerical simulation [16]. For other external stresses we sometimes found different aspects of fracture from those for the mode I stress, but they are explained by the same basic ideas as for the mode I stress. In the next section we explain our model. In Sec. III we present numerical results for mode I stress and we classify types of the fracture into three or four fracture modes giving qualitative explanations. In Sec. IV we examine the fracture for the other external stresses. In Sec. V we present conclusive discussions.

II. MODEL

We use the same model as in the previous paper [5]. Such models have been studied by many authors [22–31]. Our simulation scheme rather follows Ashurst and Hoover [22]. We collect much more data by the present simulation and give a qualitative explanation to the simulation. The equations of motion are given by

$$\frac{d\mathbf{r}_i}{dt}=\mathbf{v}_i \ , \tag{1}$$

$$\frac{d\mathbf{v}_i}{dt}=\sum_n \mathbf{F}(\mathbf{r}_i-\mathbf{r}_n) \ , \tag{2}$$

where $\mathbf{r}_i$ and $\mathbf{v}_i$ are the position and the velocity of the ith particle, which is initially placed on the ith lattice site. The lattice we employ is the triangular lattice. The summation on the right hand side of (2) is taken over nearest neighbor sites. It is equivalent to think that all particles are connected with modified harmonic springs. It was already shown that the crack propagation velocity on the triangular lattice is very similar to that in the three dimensional hexagonal closed packed lattice structure [32]. $\mathbf{F}$ is the force

$$\mathbf{F}(r)=-\frac{\mathbf{r}}{r}f(r) \ . \tag{3}$$

The scalar part $f(r)$ of the force in most cases is chosen as

$$f(r)=\begin{cases} r-1 \ , & \text{for } r\le r_0 \ , \\ 0 \ , & \text{for } r>r_0 \ , \end{cases} \tag{4}$$

where r_0 is a cut-off parameter. The above form of the interatomic force is over simplified. We shall show later that a tailed force also gives almost the same result. The equilibrium distance between nearest neighbor particles is set, being one. The above set of equations is numerically solved as follows. As the first step the velocity equation (1) is discretized

$$\mathbf{r}(t+\Delta t)=\mathbf{r}(t)+\mathbf{v}(t)\Delta t \ . \tag{5}$$

Then the force equation (2) is discretized as follows:

$$\mathbf{v}(t+\Delta t)=\mathbf{v}(t)+\mathbf{F}(t+\Delta t)\Delta t \ . \tag{6}$$

Here the force term in the right hand side of (6) is a function of $\mathbf{r}$ at time $t+\Delta t$, which is given by Eq. (5). This method is essentially equivalent to that by Verlet [33]. In fact by solving $\mathbf{v}$ in (5) and substituting it into (6) we obtain

$$\frac{\mathbf{r}(t+\Delta t)+\mathbf{r}(t-\Delta t)-2\mathbf{r}(t)}{\Delta t^2}=\mathbf{F}(t) \ ,$$

which is a time reversal symmetric equation by Verlet's algorithm. Here we have replaced t by $t-\Delta t$. Notice that in the computational program we may simply put two equations, (5) and (6), in this order. In this method the energy is conserved on the average. In this paper lengths are scaled by the equilibrium lattice constant a $(=1)$, and the velocity is scaled by the velocity of the longitudinal sound in the one dimensional system c $(=1)$. The discrete time interval Δt is chosen so that the results are insensitive to this value. Actually, values between $\Delta t=0.01$ and 0.1 have been chosen.

The system is a rectangle. A particle is placed on each site of the triangular lattice with the nearest neighbor interaction. We examine the fracture for the so-called mode I stress in detail in Sec. III. We also have done simulations for other types of external stress, i.e., mode II, mode III, and spherical external stresses, and we will discuss them later in Sec. IV.

III. CRACK PROPAGATION FOR MODE I EXTERNAL STRESS

We extensively discuss fractures for the mode I stress, which is shown in Fig. 1. In almost all cases we have done simulations with the periodic boundary condition at longer edges of the system, and the free or the solid boundary condition at shorter edges. The only exception is the case where we compute the *roughness exponent* of the crack surface. In this case we used the fixed boundary condition at longer edges of the system. One of the lattice axes is set to be parallel to the longer edges (say

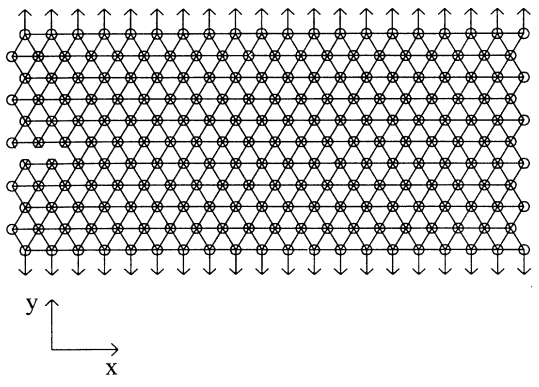

FIG. 1. Schematics of the system. Arrows indicate external stress. This type of stress is called the mode I stress. Actually the stress is imposed by setting initial lattice spacings as (7), and the periodic boundary condition is used at the longer system edges (horizontal edges) in most cases. The crack is set at one of the shorter edges until the crack starts to propagate spontaneously. Most formations of the initial crack are done with the time rate 0.1 (lattice spacings per unit time), which corresponds to the 0.1 times one dimensional sound speed. We also examined a sudden formation of the crack. However, the difference between these two conditions is not significant for the determinations of terminal crack velocities.

the x axis). Usually the magnitude of the external force is a natural external control parameter. In this paper, however, we choose an interparticle distance as a control parameter and we characterize the external force by the interparticle distance. This is because the analysis of the simulation is more conveniently done by the interparticle distance than by the external force itself. The external force is represented by the initial interparticle distances through a simple monotonic function. Let us call a bond oriented to the x axis the type 1 and others type 2. Lengths of all type 1 bonds are set shorter so that there may be no stress in the x direction initially. Lengths of type 2 bonds are set equal to $r_e(>1)$. That is, one sets

$$r=\begin{cases}(2-r_e^{-1})^{-1}, & \text{for type 1 bonds},\\ r_e, & \text{for type 2 bonds}.\end{cases} \tag{7}$$

The external force acting on the particle is, therefore, $F_x=0$ in the x direction and $F_y=(r_e-1)/(2r_e-1)\sqrt{(4r_e-3)(4r_e-1)}\approx\sqrt{3}(r_e-1)$ in the y direction (perpendicular to the x direction). The average crack surface or the crack line is parallel to the x axis and this is the stress usually called the mode I stress. Initially a crack, which is parallel to the x axis, is artificially created near a shorter edge of the system (Fig. 1). The length of the initial crack is finite or being elongated gradually before the crack begins to propagate spontaneously. Then the terminal crack propagation velocity is observed for the various system sizes $L\times N$. Here L is the width (the number of layers in the y direction) and the N is the length of the system in the x direction. We carried out simulations for $L=40$, 60, 80, 200, and $N=600$, 1000, 2000.

We examined the fracture for two values of r_0, i.e., $r_0=1.01$ and $r_0=1.1$ and for several values of r_e. These values of r_e correspond to the weak ($r_e=1.01$) and the strong ($r_0=1.1$) external stresses. We shall find that qualitative features of fractures are characterized by the parameter $(r_0-r_e)/(r_e-1)$. The quantity r_0-r_e is related to the potential barrier, and the quantity r_e-1 represents the strength of the external stress. We thus call the quantity $(r_0-r_e)/(r_e-1)$ simply the *reduced potential depth*. It will become apparent that this is an important parameter for the classification of crack propagation modes. In the present simulation we find that the crack can propagate if the values of the reduced potential depth is smaller than about ten. We note here some relations between the present simplified potential with a more realistic one. Let us consider the Lennard-Jones type interparticle potential

$$\phi(r)=\frac{1}{2m}r^{-2m}-\frac{1}{m}r^{-m}.$$

This potential function with $m=6$ is most familiar. The scalar force $f(r)$ is given by $\partial\phi/\partial r$. Let us define r_0 by $0=\partial^2\phi/\partial r_2|_{r=r_0}$ for simplicity. Then $(r_0-r_e)/(r_e-1)\approx 5$ corresponds to $r_e\approx 1.02$ for $m=6$ and $r_e\approx 1.01$ for $m=10$. On the other hand $(r_0-r_e)/(r_e-1)\approx 0.1$ corresponds to $r_e\approx 1.1$ for $m=6$ and $r_e\approx 1.07$ for $m=10$. Although a rigorous correspondence between the Lennard-Jones type potential and the truncated harmonic potential is not possible, the above estimation states that our choices of the r_e are not unrealistic.

The crack propagation velocities v are shown as functions of $(r_0-r_e)/(r_e-1)$ for $r_e=1.1$ in Fig. 2 and for $r_e=1.01$ in Fig. 3 for the interatomic force (4). The crack propagation velocity is calculated as a straight length of crack along the x axis divided by the corresponding time interval. We measure the vertical distance by assuming that all bond lengths are equal to one. Therefore, if the velocities are corrected by taking the shrink of type 1 bond into account, then they are about 10% smaller for $r_e=1.1$ and about 1% for $r_e=1.01$ than as shown in the figures. In the strong stress case we find three broad branches of the crack propagation velocity. The system size effect is seen for the critical value of the potential depth, where the crack stops propagating: For smaller system width L the critical value of the potential depth is smaller. We classified these three branches as S (supersonic), L (longitudinal), T (transverse) from the left. In the weak stress case an extra branch labeled by Z is

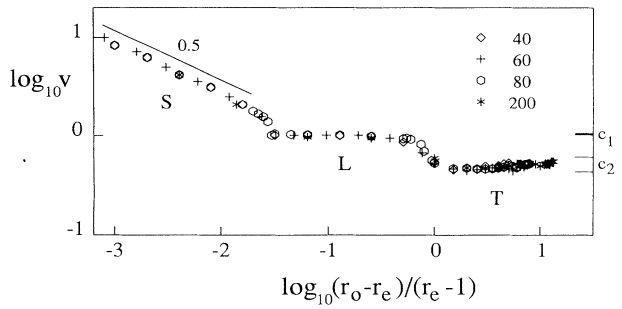

FIG. 2. The crack propagation velocity v as a function of the reduced potential depth $(r_0-r_e)/(r_e-1)$ for the mode I strong stress ($r_e=1.1$). Numbers on the figure indicate the system width L. A straight line indicates the slope -0.5. Short horizontal straight lines with symbols c_1 and c_2 indicate the upper and the lower limits of the longitudinal (0.061, 1.031) and the transverse (0.6124, 0.4430) sound velocities propagating in the x direction (along a lattice axis) evaluated in the Appendix. Symbols S, L, and T indicate the supersonic, the longitudinal, and the transverse branches, respectively.

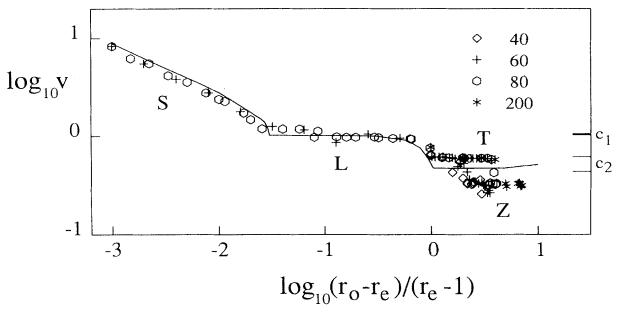

FIG. 3. Crack propagation velocity v as a function of the reduced potential depth $(r_0-r_e)/(r_e-1)$ for the mode I weak stress ($r_e=1.01$). The curve shown corresponds to the data of Fig. 2. The symbol Z indicates the zigzag branch.

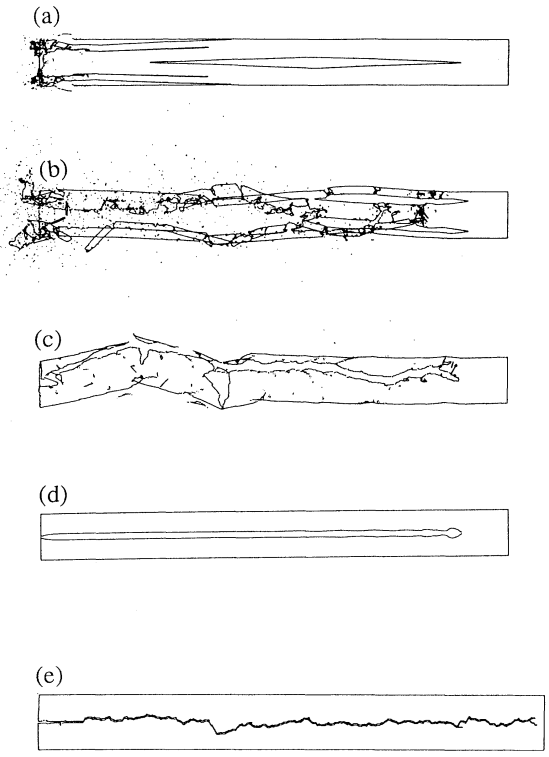

FIG. 4. Typical crack patterns for mode I stress. (a) Supersonic mode, (b) longitudinal mode, (c) and (d) transverse mode, and (e) zigzag mode. (a)–(d) $r_0-r_e=5\times10^{-4}$, 2×10^{-2}, 0.2, 0.4, respectively, in the strong stress case $r_e=1.1$, in the system of size 60×600. (e) $r_0-r_e=0.038$ in the weak stress case $r_e=1.01$ in the system of size 80×600.

found. In Fig. 4 we show typical crack patterns for typical parameter values.

A. Type S crack propagation mode

The branch S was already examined in the previous paper [5]. On this branch the crack propagation velocity exceeds the sound velocity. We here briefly review the crack propagation mechanism on this branch. When one bond is cut, the force acting on a particle becomes suddenly unbalanced, and the particle is accelerated by the force of the order r_e-1 in the direction perpendicular to the crack surface. The velocity of the particle is therefore given as a function of time t as

$$v_\perp(t)\sim(r_e-1)t \ . \tag{8}$$

Due to these motions of particles, a bond, which is connected to the moving particles, is elongated to be cut. This process continues successively to yield the crack propagation. We now assume that bonds are easily cut

$$r_0-r_e\ll r_e-1 \ , \quad (\ll 1) \ . \tag{9}$$

On the triangular lattice the bond elongation is proportional to the positional displacement of particle. Therefore, a bond cuts when the particle moves for a distance of the order r_0-r_e, and the time τ needed for the bond to cut satisfies

$$\int_0^v v_\perp(t)dt\sim(r_e-1)\int_0^\tau t dt\sim r_0-r_e \ . \tag{10}$$

Then the crack propagation velocity v is given as

$$v=\frac{1}{\tau}\sim\left[\frac{r_0-r_e}{r_e-1}\right]^{-1/2} \ . \tag{11}$$

This agrees with the simulation except for the proportionality constant, which is about $1/\sqrt{10}$ from the simulation.

B. Type L and type T crack propagation modes

The crack velocity v by the type S mode becomes smaller than the (longitudinal) sound velocity as $(r_0-r_e)/(r_e-1)$ increases, because it takes a longer time for the bond length to reach r_0. Then the crack extension is caused by sound vibrations more effectively. Let us assume that the sound propagation and the crack propagation are stationary. Let the sound amplitude near the sound propagation front be $\phi(x-ct)$, and let us assume that a bond near the tip is cut if the bond is further elongated by the amount Δr. The quantity Δr and the functional form of ϕ are time independent. The crack tip location is determined by

$$\phi(x-ct)=\Delta r \ . \tag{12}$$

This states that the crack propagation velocity v is equal to the sound velocity c in a stationary state

$$v=c \ .$$

We can find that the longitudinal and the transverse crack propagation modes appear at different regions of the reduced potential depth $(r_0-r_e)/(r_e-1)$. Namely, the longitudinal mode appears for small reduced potential depths and the transverse mode appears for large reduced potential depths. Shortly speaking, this is because the transverse sound mode more easily cuts bonds but propagates more slowly than the longitudinal sound mode. Let us explain this. First, we show that the amplitude of the transverse sound is larger than that of longitudinal sound. The relation between the amplitude A and the velocity c of the sound is given by $c^2A^2\sim$ sound energy. Thus the amplitudes by the longitudinal, A_l, and the transverse, A_t, sound modes satisfy

$$\frac{A_l}{A_t}\sim\frac{c_t}{c_l}\sim 1/2 \ , \tag{13}$$

where c_t and c_l are the transverse and the longitudinal sound velocities, respectively. For the transformation into the last side see the Appendix. Second, we show that a bond is more easily cut by the transverse sound mode than by the longitudinal sound mode if the sound amplitudes are the same in both modes. This can be easily shown. Let us consider type 2 bonds. Successive cuts of the bond of this type give rise to the crack propagation in the x direction. By the transverse sound vibration a bond is stretched by the amount $[(\sqrt{3}/2+A)^2+(1/2)^2]^{1/2}-1\sim\sqrt{3}A/2$, whereas by the longitudinal one by the amount $A/2$. By these two reasons the trans-

verse sound mode more easily cuts bonds than the longitudinal sound mode. Notice, however, that the transverse mode is not always more effective to the crack propagation than the longitudinal mode. This is because the crack by the longitudinal sound mode propagates faster than that by the transverse sound mode. Therefore, if two sound modes are simultaneously effective, then the crack formation is governed by the faster longitudinal sound mode. This is the type L region in Fig. 2 and Fig. 3. When the reduced potential depth becomes larger, the longitudinal sound mode becomes ineffective but the transverse sound mode is still effective. Then the crack propagation is done by the transverse sound mode. This is the type T region.

The limit of the crack propagation by the longitudinal sound modes may be evaluated as follows. The released energy by the cut of a bond is $(r_e-1)^2/2$ and the amplitude of the sound vibration is about (r_e-1). Thus, by assuming that the stress is not much concentrated on the crack tip, the longitudinal sound can cut bonds if

$$r_0-r_e<r_e-1 , \tag{14}$$

i.e., if

$$\frac{r_0-r_e}{r_e-1}<1 . \tag{15}$$

This gives the limit of the crack propagation by the longitudinal sound mode. The proportionality constant is only an approximation. The simulation reveals that the proportionality constant is about 1.

The same discussion can be applied to the transverse mode by assuming that the stress is not concentrated on the crack tip. The critical value for the transverse mode is larger than that for the longitudinal mode by the factor about 3.5, which is evaluated as the amplification of the sound amplitude, 2, times the amplification of the bond elongation, $\sqrt{3}$

$$\frac{r_0-r_e}{r_e-1}<2\sqrt{3}\sim 3.5 . \tag{16}$$

Up to these values the stress is assumed not to be strongly concentrated on the crack tip, and therefore the crack is not necessarily a single line. We observed that crack patterns are almost regular over the T branch in the weak external stress case ($r_e=1.01$) and on the T branch at large potential depth in the strong stress case ($r_e=1.1$). In such cases the stress may be concentrated on the crack tip for the transverse mode, and the assumption used here cannot be applied. The case of the concentrated stress will be discussed later in connection with the limit of the crack propagation.

We observed that the crack patterns of the transverse mode in the strong stress case are classified approximately into two types, i.e., irregular [Fig. 4(c)] and regular [Fig. 4(d)] ones, and also found that the crack propagation velocity is little bit smaller for the irregular crack pattern than that for the regular crack pattern. We think that the irregularity of the crack pattern may elongate the sound propagation path, and hence the crack propagation velocity becomes smaller than the sound velocity. This is consistent even in the weak stress case, i.e., the crack pattern of the transverse mode in the weak stress case is almost regular and the transverse mode in the weak stress case sometimes gives a larger crack propagation velocity than in the strong stress case.

C. Zigzag crack propagation mode

In the weak stress case there appears a completely different kind of crack pattern near the transverse branch. The crack is a single zigzag line, and the crack propagation velocity is about half of the transverse sound velocity. This type of zigzag crack may be considered to be equivalent to those examined experimentally [15] and numerically [16]. All crack propagations we have shown here start from zero temperature of a perfect crystal. We examined also the initial condition that particles have small random velocities. But results are essentially the same. Probably the randomness may come from the strong nonlinearity in the interparticle potential and the asymmetry in the initial crack. Once the randomness appears it is amplified to give the zigzag crack independently of the initial condition. Here we examine the crack propagation path length and the *roughness exponent* ζ of the crack line height. If the crack is straight, the terminal velocities by the present numerical simulation are consistent with the theoretical prediction that crack velocities are equivalent to the sound velocities [11–14]. However, for a zigzag crack the crack propagation velocity is generally smaller than the (transverse) sound velocity by a factor of about $\frac{1}{2}$. By counting the number of cut bonds we found that the total path along the crack surface is about 1.2 times the straight length of the crack in a system of size 80×600 and thus the crack propagation velocity along the crack surface is about 1.2 times the crack propagation velocity along the straight line. Such an amplification of the crack propagation velocity is insufficient to reproduce the sound velocity along the crack path. Therefore, there should be a time lag between the lattice vibration and bond cut for the zigzag crack mode: The relation (12) cannot be applied to the zigzag crack mode.

We examined the *roughness exponent* ζ of the crack surface in this system by means of the correlation function. Let the height of the surface at the position x by $y(x)$. A self-affine surface $y(x)$ is invariant for the scale transformation [17]

$$(x,y)\rightarrow(\lambda x,\lambda^{\zeta}y) . \tag{17}$$

The surface spectrum is defined by means of the autocorrelation function of y and is scaled as

$$S_k=\int\langle y(0)y(x)\rangle e^{-ikx}dx\propto k^{-1-2\zeta} . \tag{18}$$

In Fig. 5 the spectrum is shown together with an example of the crack surface profile. Only to the present purpose we used the fixed boundary condition at the longer system edges. The spectrum shown is the average of only three different spectra in the region near $r_0-r_e=0.038$ with $r_e=1.01$ and $L=80$. The straight line corresponds to the value $\zeta\sim 0.75$, which is near to those observed

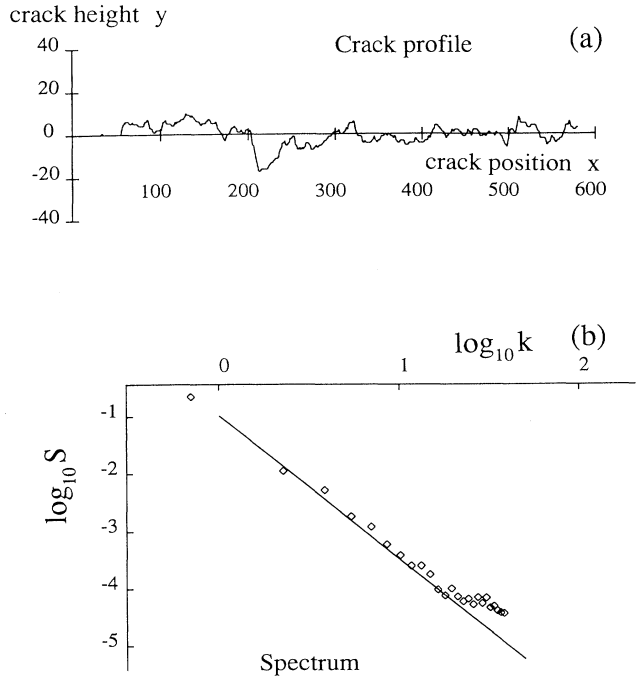

FIG. 5. (a) An example of zigzag crackline for the mode I stress. The abscissa indicates the crack position (x) and the ordinate indicates the crack height (y). Only in this case we used the fixed boundary condition. (b) Corresponding spectrum. The spectrum is the average of three different spectra for $r_e=1.01$ with $r_0-r_e=0.038$, 0.039, and 0.040. The system size is 80×600. The spectrum is calculated for 512 vertical points. The straight line corresponds to the roughness exponent $\zeta=0.75$.

values [16,20], though the number of samples is not enough to get a conclusive result. Under the periodic boundary condition we have observed generally somewhat smaller values of ζ, though crack propagation modes and the crack propagation velocities are unchanged. We have no suitable idea for this observation at this moment.

The zigzag branch cannot be observed in the strong stress case. In the weak stress case all bonds have almost the same length, and therefore the zigzag crack may easily appear. In the strong stress case, however, bonds oriented in the direction perpendicular to the stress are much shorter than other bonds, and therefore such bonds hardly cut: The crack shape is a straight line.

D. Limit of the crack propagation

When the reduced potential depth $(r_0-r_e)/(r_e-1)$ becomes larger, the lattice becomes harder to fracture. Then the stress concentrates on the crack tip and only bonds near the crack tip become unstable, and the crack extends along the most probable path yielding a single crack line. In the present simulation we use the periodic boundary conditions. For the fixed and the periodic boundary conditions the limit of the reduced potential depth for the crack propagation is system-size dependent because the lattice deformation is restricted in a finite system. We show this here. Consider a half-side infinite crack in a lattice with the width L, which is in equilibrium. Let the crack height be y at the position x from the crack tip. Generally, apart from angular dependences, the stress σ and the deformation u around the crack tip are functions of the distance R from the tip [34], i.e.,

$$\sigma(R)\sim\frac{C}{\sqrt{R}}\ ,\quad u(R)\sim C\sqrt{R}\ , \tag{19}$$

where C is a constant. At system edges this stress is equal to the external stress $(\sim r_e-1)$. Thus $\sigma(L)\sim C/\sqrt{L}\sim r_e-1$, and therefore we find $C\sim(r_e-1)\sqrt{L}$. Thus we find $\sigma(R)\sim(r_e-1)\sqrt{L/R}$, and $u(R)\sim(r_e-1)\sqrt{LR}$. Applying this deformation to the crack profile, i.e., by setting $u\to y$ and $R\to x$ we obtain

$$y\sim(r_e-1)\sqrt{Lx}\ . \tag{20}$$

Let y_1 be a vertical shift of the crack surface at $x=1$. We have

$$y_1\sim(r_e-1)\sqrt{L}\ . \tag{21}$$

This value is much larger than the amplitude of the sound vibration r_e-1. Thus we underate the sound amplitude to evaluate the elongation of the bond within the present crude approximation. Therefore, the approximate bond elongation at the crack tip is about r_e+y_1. The crack extends when a (type 2) bond at the tip becomes longer than the force range, i.e., when

$$r_e+y_1>r_0\ , \tag{22}$$

that is, when

$$\left[\frac{r_0-r_e}{r_e-1}\right]^2<L\ . \tag{23}$$

This gives the limit of the crack propagation. The above discussion is based on the straight crack shape only implicitly. Therefore, the criterion (23) may also apply to the weak stress case where the critical crack shape is zigzag. Nevertheless the application of the above discussion to the one dimensional zigzag crack is difficult, because a strong irregularity in the crack surface orientation must stop the propagation of the crack. The test of (23) was done for the strong stress case $r_e=1.1$ for systems with the length $N=600$ and various values of the width L. In all cases the cracks are gradually formed with the time

TABLE I. Critical reduced potential depths for the mode I stress for the strong external stress case ($r_e=1.1$). Shown data are critical values for which crack tips stay inside the system and cracks no longer propagate, under the periodic boundary condition at longer edges of the system and under the initial condition stated in the text. The length of the system is $N=600$.

L	40	60	80	200
$L^{-1}\left[\frac{r_0-r_e}{r_e-1}\right]^2$	0.65	0.74	0.82	0.92

rate 0.1 (lattice spacings per unit time) until the crack lengths become larger than the value of the system width L. By increasing the value of r_0 we obtain the smallest value of r_0 for which the crack tip stays inside the system and the crack does not propagate any more. We compared thus obtained values of r_0 with the predicted critical values (23). The result is shown in Table I in the case of the strong external stress $r_e=1.1$. It can be found that numerical data exhibit slight deviations from (23) about the L dependence, i.e., L may be better replaced by $L^{1.15}$.

IV. CRACK PROPAGATIONS FOR MODE II, MODE III, AND SPHERICAL EXTERNAL STRESSES

We also examined fractures for three other external stresses, i.e., mode II, mode III, and spherical external stresses. In Fig. 6 schematic explanations of these stresses are shown. The mode II stress is a shear stress. In this case we assume that all particles can move only within the lattice plane (xy plane). The mode III stress is oriented to the z direction. In this case we assume that all particles can move only in the z direction. For the spherical stress all lattice spacings are initially set equal to r_e. In this case we assume that all particles can move only within the lattice plane (xy plane). For the mode II and the mode III stresses we use a periodic boundary condition at longer system edges, whereas for the spherical stress we use a fixed boundary condition.

For the mode II and the mode III stresses bonds which are oriented to the x direction are initially set unity. For the mode II stress other two bonds within any single triangular unit are initially set as

$$r=\begin{cases}1+r_e\ , & \text{for one bond ,}\\ 1-\dfrac{r_e}{2r_e+1}\ , & \text{for the other bond .}\end{cases} \tag{24}$$

Then the net force acting on the vertex of the triangle connecting to these two bonds is parallel to the x axis. For the mode III stress bonds which are not oriented to the x direction are initially set as r_e (>1).

Figures 7–9 represent crack propagation velocities for mode II, mode III, and spherical external stresses, respectively. In this paper we briefly examine fractures in these cases.

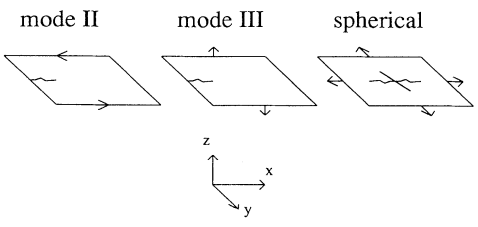

FIG. 6. Other stress types: mode II, mode III, and spherical stresses. Arrows indicate external stresses. Zigzag lines indicate cracks. For mode II stress particles are allowed to move only in the direction perpendicular to the xy plane, whereas for other stresses they are allowed to move only within the xy plane.

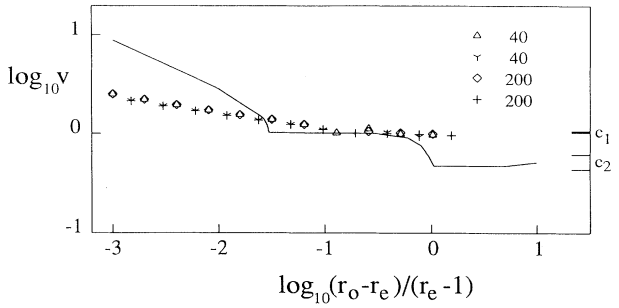

FIG. 7. Crack propagation velocity v for mode II stress as a function of the reduced potential depth $(r_0-r_e)/(r_e-1)$. Cases of $L=40$, 200, and $r_e=1.01$, 1.1 are shown in the same figure. Here small polygons are for $r_e=1.1$ and others are for $r_e=1.01$. The curve shown corresponds to the data of Fig. 2.

A. Crack propagation for mode II stress

It can be found that the crack propagation velocity is scaled by the reduced potential depth $(r_0-r_e)/(r_e-1)$. But there are two interesting differences from the case of mode I stress. (1) For the supersonic crack propagation mode, the velocity-potential relation does not obey the $\frac{1}{2}$-power law. The reason is as follows. For the mode I stress the bond cut is done by the positional displacement of a particle at the tip of the crack. Such a bond cut is directly done from bond to bond. On the other hand for the mode II stress, one bond elongates but the other bond shrinks in the one unit triangle. Therefore, the bond cut cannot be directly done from bond to bond but multiple bonds are associated to the cut of a bond. This may give a different power law (with smaller power). From the numerical result we find an approximate power law $v\sim[(r_0-r_e)/(r_e-1)]^{-0.17}$. The exponent $0.17\approx 1/6$ seems to suggest that (10) should be replaced by $\tau^6\propto r_0-r_e$. Three bonds collaboration may explain this. (2) We cannot observe the transverse mode of the crack

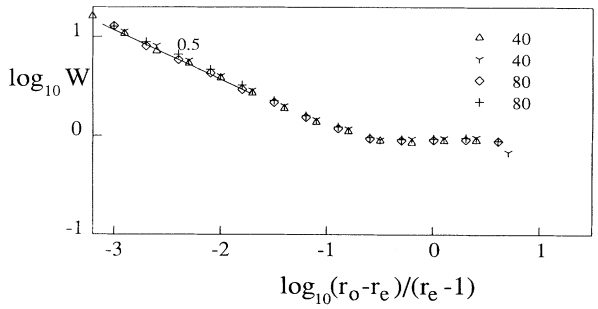

FIG. 8. Crack propagation velocity (modified) for mode III stress as a function of the reduced potential depth $(r_0-r_e)/(r_e-1)$. Cases of $L=40$, 80, and $r_e=1.01$, 1.1 are shown in the same figure. Here small polygons are for $r_e=1.1$ and others are for $r_e=1.01$. The vertical axis indicates the logarithm of $W\equiv v/\sqrt{3(r_e-1)/2}$ with the crack propagation velocity v. Here the sound velocity in this case is given by $\sqrt{3(r_e-1)/2}$. The straight line indicates a slope -0.5.

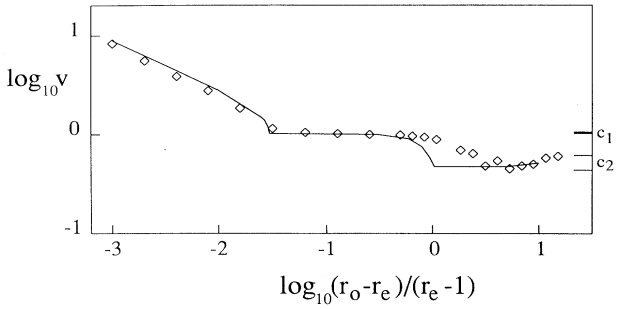

FIG. 9. Crack propagation velocity v for spherical stress as a function of the reduced potential depth $(r_0-r_e)/(r_e-1)$ in the case $r_e=1.1$ with the potential represented by (4). The system size is 700×700. The curve shown corresponds to data of Fig. 2.

propagation, and hence we cannot observe the zigzag crack propagation mode. The reason is not obvious at this moment.

B. Crack propagation for mode III stress

A remarkable difference of the crack propagation velocity from those for other stress modes is that the crack propagation velocity is a function not only of the reduced potential depth $(r_0-r_e)/(r_e-1)$ but also of r_e-1. But even in this case the above idea can apply to the present case by slightly modifying it. Notice that the z component of the restoring force F_z by a single bond elongation is given as

$$F_z=-(r_e-1)\Delta z \ ,$$

where the Δz is the relative positional displacement along the z axis. From this the sound propagation velocity can be calculated. We can find that the longitudinal and the transverse sounds propagating in the x direction have the same velocity $\sqrt{3(r_e-1)/2}$ in this case. By rescaling the crack propagation velocity by this sound velocity we find that the crack propagation velocity can be represented by a single master curve as in other stress cases. In Fig. 8 the quantity W is defined by $W\equiv v/\sqrt{3(r_e-1)/2}$. In this case we observed only one flat branch, where the crack propagation velocity is smaller than the sound velocity only by the amount about 10% or less.

C. Crack propagation for spherical stress

All bonds are initially set to the same length r_e, and the spherically symmetric velocities are given to particles near the center of the system. The same analysis was also done in the previous paper within a restricted parameter region [5]. Cracks patterns are spherically symmetric. The crack propagation velocity v is calculated by observing the outermost crack tip. The crack propagation velocity is shown in Fig. 9. We can find that there are three branches (S,L,T) as in the case of mode I stress. The crack propagation velocity on the type T branch increases as the $(r_0-r_e)/(r_e-1)$ increases up to the bulk transverse sound velocity.

V. CONCLUSIONS AND REMARKS

We have studied the mechanics of fracture using a two dimensional model. This model is simplified in two respects. First, the potential between particles is a simplified truncated harmonic potential. But it is shown below that the crack propagation velocity is not much affected by the potential form. Second, interactions are limited between definite partners which are set initially between nearest neighbor sites. Therefore, most secondary collisions such as cluster-cluster collision and particle-cluster collisions are not accounted for in the present study. Because the crack-tip formation is the first fracture process, such secondary processes are not important. Therefore, the model is sufficient to the present purpose. We now summarize our main conclusions. The following (1)–(3) are for the mode I stress.

(1) When the crack propagation velocity is represented as a function of the reduced potential depth $(r_0-r_e)/(r_e-1)$, it has three or four branches. Two of them are related to the longitudinal and the transverse sound modes. When the crack propagation is stationary, it is natural that the crack propagation velocity is equal to the sound velocity [see (12)]. When there are many sound modes, many corresponding crack propagation modes may appear as the potential depth varies. For a small reduced potential depth the crack propagation velocity exceeds the sound velocity forming a typical branch. In this case a crack is formed not by the sound vibration but mainly by the imposed external stress. These crack propagation mechanisms are not affected by a slight modification of the interparticle force. Instead of the force given by (4), we also examined crack propagation velocity for the following force

$$f(r)=\begin{cases}(r-1) \ , & \text{for } r\le\frac{1}{2}(r_e+r_0) \ , \\ \frac{1}{2}(r_e+r_0)-1 \ , & \text{for } \frac{1}{2}(r_e+r_0)<r\le r_0 \ , \\ 0 \ , & \text{for } r>r_0 \ . \end{cases} \tag{25}$$

This force has a flat part at the tail. The cut of the bond is defined also by the bond length which is larger than r_0. The numerical result for $r_e=1.1$ is shown in Fig. 10.

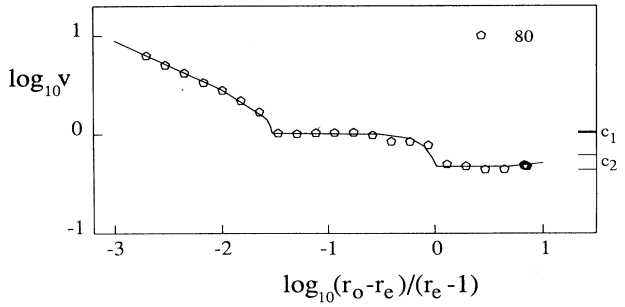

FIG. 10. The crack propagation velocity v for mode I strong stress $(r_e=1.1)$ with the tailed potential represented by (25). The horizontal axis is the logarithm of the same reduced potential depth $(r_0-r_e)/(r_e-1)$ defined for (7). We used the system with $L=80$. The curve shown corresponds to the data of Fig. 2.

There are still three types of branches S, L and T, which are almost the same as those for the interparticle force (4). This means that the physical picture based on the sound modes is suitable.

(2) In the weak stress case a single zigzag crack appears before the crack stops propagating. The crack propagation velocity is in general smaller than the sound velocity by a factor about $\frac{1}{2}$. Even if the crack propagation velocity is measured along the crack surface, the effective crack propagation velocity is smaller than the surface sound velocity. The crack propagation velocity is almost constant in a finite range of the reduced potential depth, and thus gives the fourth branch of the crack propagation velocity. In the case of zigzag crack the crack surface is fractal exhibiting the roughness exponents about 0.75. This branch cannot be observed in the strong stress case. This is because the bonds oriented to the direction perpendicular to the external stress must shrink in the strong stress case.

(3) The limit of the crack propagation depends on the system width L under the periodic boundary condition. A finite size scaling (21) is derived and shown that this scaling is supported by the numerical simulation. According to this analysis the limiting potential depth becomes larger as the system width L becomes larger.

(4) We have examined simulations for the other types of stress, i.e., the mode II and the mode III stresses and the spherical stress. These simulations provided new aspects of the fracture. But such aspects can be well explained based on or by extending several ideas shown for the mode I stress.

ACKNOWLEDGMENTS

This work is supported by the Japanese Ministry of Education, Science, and Culture.

APPENDIX: SOUND VELOCITIES

Velocities of sounds propagating on the triangular lattice can be calculated by a standard technique. Here we give only the result. Let the x axis be parallel to one of the lattice axes and the y axis be perpendicular to the x axis. Let $\mathbf{k}=(k_x,k_y)$ be the wave vector of the sound. The bulk sound velocity c is given by

$$c^2=\frac{3}{4}\left[1\pm\left[1-(3/4k^4)(k_x^2-k_y^2)^2\right]^{1/2}\right].$$

Here the plus sign indicates the longitudinal sound velocity, and the minus sign the transverse sound velocity. The explicit values of the velocity of the sound propagating along the x axis are $c_l=3/(2\sqrt{2})\approx 1.061$ for the longitudinal mode, and $c_t=\sqrt{3}/(2\sqrt{2})\approx 0.6124$ for the transverse mode.

In the presence of the crack surface, surface sound modes appear. A nonrigorous but a simplified method of evaluating lower bounds of surface sound velocities is as follows. Two bonds per atom are cut on the surface in the triangular lattice. Thus the restoring force of the particle motion on the surface is reduced compared to the bulk system. We approximate the restoring force of the surface sound by setting the corresponding force constant to be half of the bulk value (the force constant of the bond parallel to the x axis, i.e., the crack surface, is unchanged). This underestimates the restoring force, since deeper sites reduce to bulk sites. By considering the bulk sound motion with this approximate restoring force we obtain the underestimated surface sound velocity. This gives $\sqrt{17}/4\approx 1.031$ for the longitudinal mode and $\sqrt{3}/4\approx 0.4330$ for the transverse mode. The longitudinal surface sound velocity is almost the same as the bulk value. The true transverse surface sound (the Rayleigh sound) velocity $\frac{1}{2}\sqrt{3-\sqrt{3}}\approx 0.5630$ [35] lies between the above two transverse sound velocities. It is to be noted that the surface sound velocity in a system with a finite width is smaller than the Rayleigh sound velocity but should be larger than the lower bound $\sqrt{3}/4$ given above.

[1] *Statistical Models for the Fracture of Disordered Media,* edited by H. J. Herrman and S. Roux (North-Holland, Amsterdam, 1990).
[2] M. Hirata, Sci. Pap. Inst. Phys. Chem. Res. (Japan) **16**, 172 (1931).
[3] A. Yuse and M. Sano, Nature **362**, 329 (1993).
[4] Y-h. Taguchi, Mater. Sci. Eng. A **176**, 295 (1994).
[5] H. Furukawa, Prog. Theor. Phys. **90**, 949 (1994).
[6] Y. Hayakawa, Phys. Rev. E **49**, 1804 (1994); **50**, R1748 (1994).
[7] S. Sasa, K. Sekimoto, and H. Nakanishi, Phys. Rev. E **50**, R1733 (1994).
[8] M. Marder, Nature **362**, 295 (1933).
[9] J. S. Langer, Rev. Mod. Phys. **52**, 1 (1980).
[10] *Random Fluctuations and Pattern Growth: Experiments and Models,* edited by H. E. Stanley and N. Ostrowsky (Kluwer Academic, Dordrecht, 1988).
[11] L. B. Freund, *Dynamical Fracture Mechanics* (Cambridge Univ. Press, New York, 1990).
[12] J. S. Langer, Phys. Rev. Lett. **70**, 3592 (1993); Phys. Rev. A **46**, 3123 (1992).
[13] J. S. Langer and H. Nakanishi, Phys. Rev. B **48**, 439 (1993).
[14] H. Nakanishi, Phys. Rev. E **49**, 5412 (1994).
[15] J. Fineberg, S. P. Gross, M. Marder, and H. L. Swinney, Phys. Rev. Lett. **67**, 457 (1991); Phys. Rev. B **45**, 5146 (1992).
[16] F. F. Abraham, D. Brodbeck, R. A. Rafey, and W. E. Rudge, Phys. Rev. Lett. **73**, 272 (1994).
[17] B. B. Mandelbroit, D. E. Passoja, and A. J. Paullay, Nature (London) **308**, 721 (1984).
[18] E. Bouchaud, G. Lapasset, and J. Planés, Europhys. Lett. **13**, 73 (1990).
[19] A. Hansen, E. L. Hinrichsen, and S. Roux, Phys. Rev. Lett. **66**, 2476 (1991).
[20] T. Engøy, K. J. Måløy, A. Hansen, and S. Roux, Phys. Rev. Lett. **73**, 834 (1994).
[21] A. A. Griffith, Philos. Trans. R. Soc. London, Ser. A **221**,

163 (1920).
[22] W. T. Ashurst and W. G. Hoover, Phys. Rev. B **14**, 1465 (1976).
[23] J. H. Weiner and M. Pear, J. Appl. Phys. **46**, 2398 (1975).
[24] R. Thomson, C. Hsieh, and V. Rana, J. Appl. Phys. **42**, 3154 (1971).
[25] A. Paskin, A. Gohar, and G. J. Dienes, Phys. Rev. Lett. **44**, 940 (1980).
[26] Y. Termonia and P. Meakin, Nature **320**, 429 (1986).
[27] A. J. Skejltorp and P. Meakin, Nature **335**, 424 (1988).
[28] P. Meakin, Science **252**, 226 (1991).
[29] W. A. Curtin and H. Scher, J. Mater. Res. **5**, 554 (1990).
[30] Y. Mori, K. Kaneko, and M. Wadati, J. Mater. Sci. **26**, 6027 (1991).
[31] M. Marder and X. Liu, Phys. Rev. Lett. **71**, 2417 (1993).
[32] H. Furukawa, Prog. Theor. Phys. **93**, 835 (1995).
[33] See Ref. [22].
[34] G. R. Irwin, Trans. ASME, J. Appl. Mech. **24**, 361 (1957).
[35] Lord Rayleigh, Proc. London Math. Soc. **17**, 4 (1887).